7C.3 SHOCK-LIKE STRUCTURES IN THE TROPICAL CYCLONE BOUNDARY LAYER

Christopher J. Slocum *
Cooperative Institute for Research in the Atmosphere, Colorado State University, Fort Collins, Colorado

1. INTRODUCTION

Figure 1 shows the tangential, radial, and vertical components of the velocity sampled by the NOAA WP-3D Orion near an altitude of 450 m for Hurricanes Allen on 6 August 1980 and Hugo 15 September 1989. While the storms have a similar maximum tangential wind, several striking differences stand out: radius of maximum wind, abruptness and magnitude of the change in the radial and tangential velocities in the core, and the broadness of the wind field. Because of each storm's intensity and unique characteristics, the observations have been the center of several studies and have furthered our understanding of inner core processes (Jorgensen 1984; Marks et al. 2008). In examining these storms, the authors focused on small-scale features and asymmetric processes such as barotropic instability (Schubert et al. 1999). In addition to prior explanations, it is reasonable to ask if there is an axisymmetric, boundary layer argument also at work.

Seeking an answer to inner-core vortex structure questions, Haurwitz (1935, 1936) extended Ekman theory to include curvature effects with the goal of providing an explanation for why tropical cyclones have an eye. More recently, modeling work has grappled with the roles of the linear and nonlinear terms (Kepert 2001; Smith and Vogl 2008; Bryan and Rotunno 2009). To understand the dynamics that arise from the nonlinear terms and how these terms address structure questions, Williams et al. (2013), Slocum et al. (2014), Schubert et al. (2017), and Slocum (2018) examined the effects of the embedded Burgers' equation — the simplest equation to combine both the effects of nonlinear propagation and diffusion (Bateman 1915; Burgers 1948; Whitham 1974; LeVeque 1992). The combined effects influence how information flows within the system in such a way that an initially smooth wind field can evolve into sharp gradients (i.e., shocks). The formation of shocks from the tropical cyclone boundary layer equations offers an axisymmetric explanation for the abrupt 60 m s^{-1} change in tangential velocity and 35 m s^{-1} change in radial inflow observed in Hugo (see Williams et al. 2013).

While the existence and formation of shock-like features seem consistent with the Hurricane Hugo (1989) observations, how do the nonlinear terms influence the boundary layer flow for other systems such as Hurricane Allen? To address this question, a slab boundary layer model is used for various gradient wind profiles that represent weak to strong vortices that range from broad to narrow in terms of wind field extent.

*Corresponding author address: Christopher J. Slocum, Cooperative Institue for Research in the Atmosphere, Colorado State University, 1375 Campus Delivery, Fort Collins, CO 80523-1375;
E-mail: Christopher.Slocum@colostate.edu.

2. SLAB AND LOCAL BOUNDARY LAYER MODELS

This work considers an axisymmetric, depth-averaged, f-plane boundary layer model. The flow in this model is driven by the radial pressure gradient force from the overlying fluid — expressed by the gradient balanced tangential wind $\upsilon_{\rm gr}(r)$. The governing system of differential equations takes the form

$$\frac{\partial u}{\partial t}+u\frac{\partial u}{\partial r}+w^{-}\left(\frac{u}{h}\right)= \left(f+\frac{\upsilon+\upsilon_{\rm gr}}{r}\right)(\upsilon-\upsilon_{\rm gr})-c_{D}(U)U\frac{u}{h}+K\frac{\partial}{\partial r}\left(\frac{\partial(ru)}{r\partial r}\right), \tag{1}$$

$$\frac{\partial \upsilon}{\partial t}+u\left(f+\frac{\partial \upsilon}{\partial r}+\frac{\upsilon}{r}\right)+w^{-}\left(\frac{\upsilon-\upsilon_{\rm gr}}{h}\right)= -c_{D}(U)U\frac{\upsilon}{h}+K\frac{\partial}{\partial r}\left(\frac{\partial(r\upsilon)}{r\partial r}\right), \tag{2}$$

$$w=-h\frac{\partial(ru)}{r\partial r} \quad \text{and} \quad w^{-}=\frac{1}{2}(|w|-w), \tag{3}$$

where

$$U=0.8(u^{2}+\upsilon^{2})^{1/2} \tag{4}$$

is the wind speed at 10 m height, $f=5\times10^{-5}$ s^{-1} is the constant Coriolis parameter, $K=1000$ m^2 s^{-1} is the constant horizontal diffusivity, $h=1000$ m is the depth of the slab, and $c_D(U)$ is the drag coefficient.

Two local models can be derived from the full slab. The first local model (LM1) neglects the time derivative, horizontal diffusion, radial advection term in the radial equation, and vertical advection terms in addition to making selective use of the gradient balance approximation. The second local model (LM2) neglects the surface drag terms in the radial momentum equation so that $\upsilon=\upsilon_{\rm gr}(r)$ — essentially the same boundary layer used by Ooyama (1969a). The steps for deriving the solutions for LM1 and LM2 are detailed in Slocum (2018).

For the gradient balanced tangential wind profile in the overlying fluid, this work uses the double Gaussian profile

$$\upsilon_{\rm gr}(r)=\frac{\Gamma}{2\pi r}\Big[1-\frac{\gamma\Gamma_1}{\Gamma}\left(1+h_1\frac{r^2}{a_1^2}\right)e^{-r^2/a_1^2} -\frac{(1-\gamma)\Gamma_2}{\Gamma}\left(1+h_2\frac{r^2}{a_2^2}\right)e^{-r^2/a_2^2}\Big], \tag{5}$$

where Γ_1 and Γ_2 are the strength of the circulation, a_1 and a_2 are the radial extent of the vortex, $h_1=0.6$ and $h_2=1$ are the hollowness parameters, and $\gamma=0.5$ is the weighting between the vortices.

Figure 2 shows the tangential (top row), radial (middle row), and vertical (bottom row) components of the wind produced by the slab (orange curve), LM1 (dark blue curve), and LM2 (light blue curve) for three vortices: a) a weak vortex, b) a strong, narrow vortex, and c) a strong,

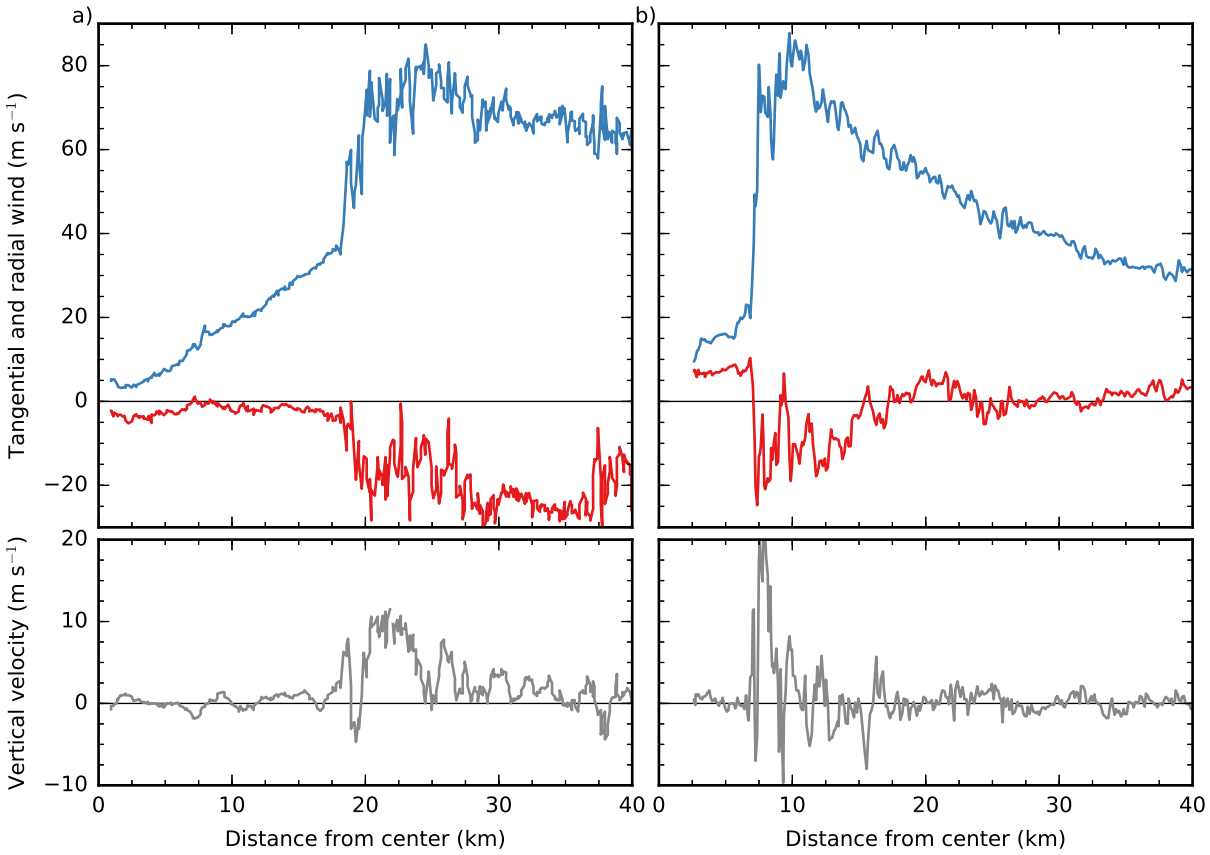

FIG. 1. Flight-level winds from aircraft reconnaissance from the NOAA WP-3D Orion for Hurricanes a) Allen on 6 August 1980 and b) Hugo on 15 September 1989. The flight-level altitude for both storms is near 450 m. The top row shows the tangential winds v (blue curves) and radial winds u (red curves) and the bottom row is the vertical velocity w (gray curve).

broad vortex. In the weak vortex case, the radial inflow maximum is only slightly displaced radially inward from the maximum in LM1 and LM2. In contrast, for the strong, narrow vortex, the magnitude of the inflow between the full slab and LM1 are the same, but LM2 produces drastically stronger inflow. Also, the placement of the updraft shifts from inside of the radius of maximum wind in the full slab to outside for both local models — a result consistent with Ooyama (1969b). In the output from the slab model for the strong, broad vortex, there are two maxima in the radial and vertical velocities — a feature not adequately captured by the local models. The subpression of the inner inflow maximum also stands out incomparison to the narrow vortex case.

3. DISCUSSION

In this work, different gradient balanced tangential wind profiles are explored to understand the effect of the nonlinear terms and shock formation. In the weak vortex case, the inflow generated by the agradient forcing term is insufficient to overcome the dissipative effects — consistent with the line-symmetric metaphor modeling results by Schubert et al. (2017) and Slocum (2018) — resulting in a scenario where a shock does not form and the local models capture most of the structure. In the stronger cases, the underlying assumptions made in formulating the local models break down, a shock develops, and the updraft shifts into a region of high inertial stability in the slab model. As the vortex wind field broadens — a scenario that foreshadows eyewall replacement (Rozoff et al. 2012), a secondary inflow maximum develops in all models. However, the slab model creates a scenario where the outer maximum is favored suggesting that shock dynamics play a critical role in eyewall replacement. The results shown here indicate that there is a critical interplay between the overlying fluid and the nonlinear terms, which is critical to not only understanding differences between broad and weak storms, but also to storm evolution by placing the frictional updraft in the high inertial stability region or cutting off inflow during eyewall replacement.

Acknowledgments

The author would like to thank Wayne Schubert for his comments. This research has been supported by NSF

under Grants AGS-1546610 and AGS-1601623 and the Hurricane Forecast Improvement Program (HFIP).

REFERENCES

Bateman, H., 1915: Some recent researches on the motion of fluids. *Mon. Wea. Rev.*, **43**, 163–170, doi:10.1175/1520-0493(1915)43⟨163:SRROTM⟩2.0.CO;2.

Bryan, G. H., and R. Rotunno, 2009: The maximum intensity of tropical cyclones in axisymmetric numerical model simulations. *Mon. Wea. Rev.*, **137**, 1770–1789, doi:10.1175/2008MWR2709.1.

Burgers, J. M., 1948: A mathematical model illustrating the theory of turbulence. *Adv. Appl. Mech.*, **1**, 171–199, doi:10.1016/S0065-2156(08)70100-5.

Haurwitz, B., 1935: On the change of the wind with elevation under the influence of viscosity in curved air currents. *Gerlands Beitr. Geophys.*, **45**, 243–267.

Haurwitz, B., 1936: Supplementary to: On the change of the wind with elevation under the influence of viscosity in curved air currents. *Gerlands Beitr. Geophys.*, **47**, 203–205.

Jorgensen, D. P., 1984: Mesoscale and convective-scale characteristis of mature hurricanes. Part II: Inner core structure of Hurricane Allen (1980). *J. Atmos. Sci.*, **41**, 1287–1311, doi:10.1175/1520-0469(1984)041⟨1287:MACSCO⟩2.0.CO;2.

Kepert, J. D., 2001: The dynamics of boundary layer jets within the tropical cyclone core. Part I: Linear theory. *J. Atmos. Sci.*, **58**, 2469–2484, doi:10.1175/1520-0469(2001)058⟨2469:TDOBLJ⟩2.0.CO;2.

LeVeque, R. J., 1992: *Numerical methods for conservation laws*. Birkhäuser, 228 pp.

Marks, F. D., P. G. Black, M. T. Montgomery, and R. W. Burpee, 2008: Structure of the eye and eyewall of Hurricane Hugo (1989). *Mon. Wea. Rev.*, **136**, 1237–1259, doi:10.1175/2007MWR2073.1.

Ooyama, K., 1969a: Numerical simulation of the life cycle of tropical cyclones. *J. Atmos. Sci.*, **26**, 3–40, doi:10.1175/1520-0469(1969)026⟨0003:NSOTLC⟩2.0.CO;2.

Ooyama, K., 1969b: Numerical simulation of tropical cyclones with an axi-symmetric model. *Proc. Third Symposium on Numerical Weather Prediction*, Tokyo, WMO/IUGG, 81–88.

Rozoff, C. M., D. S. Nolan, J. P. Kossin, F. Zhang, and J. Fang, 2012: The roles of an expanding wind field and inertial stability in tropical cyclone secondary eyewall formation. *J. Atmos. Sci.*, **69**, 2621–2643, doi:10.1175/JAS-D-11-0326.1.

Schubert, W. H., M. T. Montgomery, R. K. Taft, T. A. Guinn, S. R. Fulton, J. P. Kossin, and J. P. Edwards, 1999: Polygonal eyewalls, asymmetric eye contraction, and potential vorticity mixing in hurricanes. *J. Atmos. Sci.*, **56**, 1197–1223, doi:10.1175/1520-0469(1999)056⟨1197:PEAECA⟩2.0.CO;2.

Schubert, W. H., C. J. Slocum, and R. K. Taft, 2017: Basic concepts involved in tropical cyclone boundary layer shocks. [Available online at http://arxiv.org/abs/1709.00101.], 29 pp.

Slocum, C. J., 2018: The role of inner-core and boundary layer dynamics on tropical cyclone structure and intensification. Ph.D. thesis, Colorado State University, 123 pp.

Slocum, C. J., G. J. Williams, R. K. Taft, and W. H. Schubert, 2014: Tropical cyclone boundary layer shocks. [Available online at http://arxiv.org/abs/1405.7939.], 19 pp.

Smith, R. K., and S. Vogl, 2008: A simple model of the hurricane boundary layer revisited. *Quart. J. Roy. Meteor. Soc.*, **134**, 337–351, doi:10.1002/qj.216.

Whitham, G. B., 1974: *Linear and nonlinear wave*. Wiley, 636 pp.

Williams, G. J., R. K. Taft, B. D. McNoldy, and W. H. Schubert, 2013: Shock-like structures in the tropical cyclone boundary layer. *J. Adv. Model. Earth Syst.*, **5**, 338–353, doi:10.1002/jame.20028.

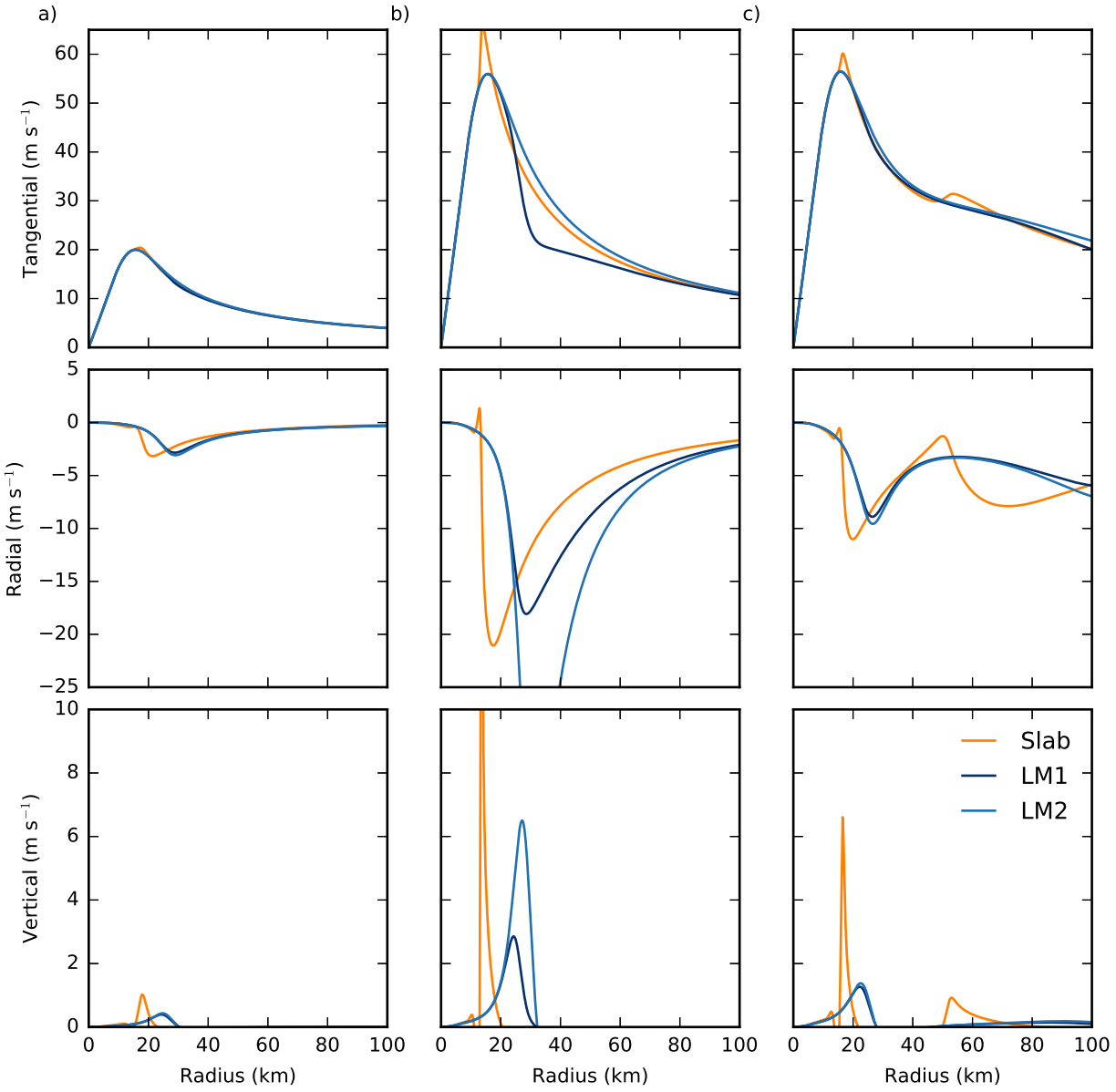

FIG. 2. Solutions for a) a weak vortex ($\Gamma_1 = 5$ 10^6 m^2 s^{-1}, $\Gamma_2 = 0$, $a_1 = 10$ km, $a_2 = 0$ km, $v_{\mathrm{gr,max}} \approx 20$ m s^{-1}, $r_{\mathrm{gr,max}} \approx 15.8$ km), b) a strong , narrow vortex ($\Gamma_1 = 14$ 10^6 m^2 s^{-1}, $\Gamma_2 = 0$ 10^6 m^2 s^{-1}, $a_1 = 10$ km, $a_2 = 0$ km, $v_{\mathrm{gr,max}} \approx$56 m s^{-1}, $r_{\mathrm{gr,max}} \approx$15.8 km), and c) a strong, broad vortex ($\Gamma_1 = 14$ 10^6 m^2 s^{-1}, $\Gamma_2 = 14$ 10^6 m^2 s^{-1}, $a_1 = 10$ km, $a_2 = 45$ km, $v_{\mathrm{gr,max}} \approx$56 m s^{-1}, $r_{\mathrm{gr,max}} \approx$15.8 km). The rows in each panel are the tangential velocity v, the radial velocity u, and the vertical velocity w for the slab boundary layer model (orange curve) and local models LM1 (dark blue curve) and LM2 (light blue curve).